arXiv:1608.06064v2 [cond-mat.supr-con] 13 Dec 2016

Superconductivity and electronic fluctuations in $Ba_{1-x}K_xFe_2As_2$ studied by Raman scattering

S.-F. Wu,[1,2] P. Richard,[2,3,4,*] H. Ding,[2,3,4] H.-H. Wen,[5,6] Guotai Tan,[7] Meng Wang,[8] Chenglin Zhang,[7] Pengcheng Dai,[7] and G. Blumberg[1,9,†]

[1] *Department of Physics and Astronomy, Rutgers University, Piscataway, NJ 08854, USA*
[2] *Beijing National Laboratory for Condensed Matter Physics, and Institute of Physics, Chinese Academy of Sciences, Beijing 100190, China*
[3] *School of Physical Sciences, University of Chinese Academy of Sciences, Beijing 100190, China*
[4] *Collaborative Innovation Center of Quantum Matter, Beijing, China*
[5] *National Laboratory of Solid State Microstructures and Department of Physics, Nanjing University, Nanjing 210093, China*
[6] *Collaborative Innovation Center of Advanced Microstructures, Nanjing University, China*
[7] *Department of Physics and Astronomy, Rice University, Houston, TX 77005, USA*
[8] *Department of Physics, University of California, Berkeley, California 94720, USA*
[9] *National Institute of Chemical Physics and Biophysics, 12618 Tallinn, Estonia*

(Dated: December 14, 2016)

Using polarization-resolved electronic Raman scattering we study under-doped, optimally-doped and over-doped $Ba_{1-x}K_xFe_2As_2$ samples in the normal and superconducting states. We show that low-energy nematic fluctuations are universal for all studied doping range. In the superconducting state, we observe two distinct superconducting pair breaking peaks corresponding to one large and one small superconducting gaps. In addition, we detect a collective mode below the superconducting transition in the B_{2g} channel and determine the evolution of its binding energy with doping. Possible scenarios are proposed to explain the origin of the in-gap collective mode. In the superconducting state of the under-doped regime, we detect a re-entrance transition below which the spectral background changes and the collective mode vanishes.

I. INTRODUCTION

Multi-band systems often exhibit complex phase diagrams. Host to spin-density-wave and nematic order in the underdoped regime and critical behavior for dopings near the maximum superconducting (SC) transition temperature T_c, the Fe-based superconductors provide a play-ground for studying many-body electronic interactions and emerging collective modes. Although still debated, many theories claim that the unconventional superconductivity of the Fe-based superconductors itself derives from effective low-energy electronic interactions [1–3], thus justifying the quest for a thorough understanding of their nature.

For the high-T_c cuprate superconductors, one of the hallmarks of unconventional superconductivity was the observation of a neutron spin resonance mode appearing in the SC state at the antiferromagnetic wave vector **Q** [4–12]. Interestingly, a similar magnetic resonance mode has also been detected at 14 meV in the archetype Fe-based superconductor $Ba_{0.6}K_{0.4}Fe_2As_2$ [13, 14]. Corresponding signatures of bosonic modes were also detected by single electron spectroscopies such as angle-resolved photoemission spectroscopy (ARPES) [15] and scanning tunneling spectroscopy (STS) [16]. A sharp mode at 10 meV has also been reported in the parent compound [17]. These observations confirm the existence of collective excitations in the Fe-based superconductors. However, due to the complex coupling between the spin, charge, lattice and orbital degrees of freedom [18], their origin is more difficult to interpret than for the simpler single band cuprates.

For the Fe-based superconductors, electronic Raman spectroscopy, which directly couples to spin singlet charge excitation at zero momentum, has recently revealed in-gap collective modes which have never been reported for the cuprates or conventional superconductors. For example, strong and sharp in-gap modes were observed for the $NaFe_{1-x}Co_xAs$ (the Na-111 electron-doped family) superconductors in both the fully-symmetric and the quadrupolar channels [19]. In-gap Raman active modes were also reported for the electron-doped $Ba(Fe_{1-x}Co_x)_2As_2$ family [20] and for hole-doped $Ba_{0.6}K_{0.4}Fe_2As_2$ [21–23]. While several interpretations for these remarkable resonances were proposed [19, 20, 24–34], the origin of the electronic interactions leading to these in-gap resonances for multi-band Fe-based superconductors remains unresolved and calls for more extensive studies.

In this work we use polarization-resolved Raman spectroscopy to study the $Ba_{1-x}K_xFe_2As_2$ family of superconductors as function of the hole-doping, in both the normal and SC states. We demonstrate that the critical quadrupolar nematic charge fluctuations of XY-symmetry persist across the entire phase diagram, similar to the family of electron-doped materials [19]. In addition, nematic fluctuations of $(X^2\text{-}Y^2)$-symmetry have also been detected. In the SC state, we observe pair-breaking coherence peaks at energies consistent with the

* p.richard@iphy.ac.cn
† girsh@physics.rutgers.edu

values reported by single-particle spectroscopies. In addition, we study the evolution of the binding energy of the XY-symmetry in-gap collective mode with doping. We report a re-entrance behavior from the four-fold symmetry broken to the four-fold symmetry preserved phase in the SC state of the underdoped $Ba_{0.75}K_{0.25}Fe_2As_2$.

In Sec. II, we introduce the sample preparation and the Raman experiments. We present our Raman results for three dopings in the A_{1g}, B_{1g} and B_{2g} symmetry channels in Sec. III A and Sec. III B for the normal and SC states, respectively. In Sec. IV, we discuss possible scenarios for the origin of the in-gap mode. The results are summarized in Sec. V.

II. EXPERIMENT

Single crystals of $Ba_{1-x}K_xFe_2As_2$ (x = 0.25, 0.4 and 0.6, with T_c values of 31 K, 38 K and 25 K, respectively) were grown by the self-flux method as described in Ref. [35]. These samples are labeled UD (underdoped), OPD (optimally-doped) and OD (over-doped), respectively. The crystals used for Raman scattering were cleaved in nitrogen gas atmosphere and positioned in a continuous flow liquid helium optical cryostat. Since the optimally-doped sample was cleaved twice, the corresponding sets of data are labeled "OPD#1" and "OPD#2".

The measurements presented here were performed in a quasi-back scattering geometry along the c-axis using a Kr^+ ion laser. Except for inset of of Fig. 5(c), for which the 752 nm (1.65 eV) laser line was used, all data were recorded with 647.1 nm (1.92 eV) excitation. The incident laser beam was focused onto a 50×100 μm^2 spot on the ab-surface, with an incident power smaller than 10 and 3 mW for measurements in the normal and SC states, respectively. The scattered light was collected and analyzed by a triple-stage Raman spectrometer designed for high-stray light rejection and throughput, and recorded using a liquid nitrogen-cooled charge-coupled detector. The Raman spectra were corrected for the spectral responses of the spectrometer and detector. The temperature has been corrected for the laser heating.

In this manuscript, we define X and Y along the 2 Fe unit cell crystallographic axes a and b (at 45° degrees from the Fe-Fe direction) in the tetragonal phase, whereas X′ and Y′ are along the Fe-Fe directions, as shown is Figs. 1(a)-1(b).

For crystals with the D_{4h} point group symmetry, the XX, X′Y′ and XY Raman geometries probe the A_{1g}+B_{1g}, A_{2g} + B_{1g} and A_{2g}+ B_{2g} channels, respectively [36]. Assuming the same featureless luminescence background I_{BG} for all polarization geometries and that the A_{2g} response is negligible, the imaginary part of the Raman susceptibility in the A_{1g} channel can be obtained by subtracting the X′Y′ spectrum from the XX spectrum and then dividing by the Bose-Einstein factor $1 + n(\omega, T)$. The imaginary part of the Raman susceptibility in the B_{1g} and B_{2g} channels can be obtained from X′Y′ and XY spectra, respectively.

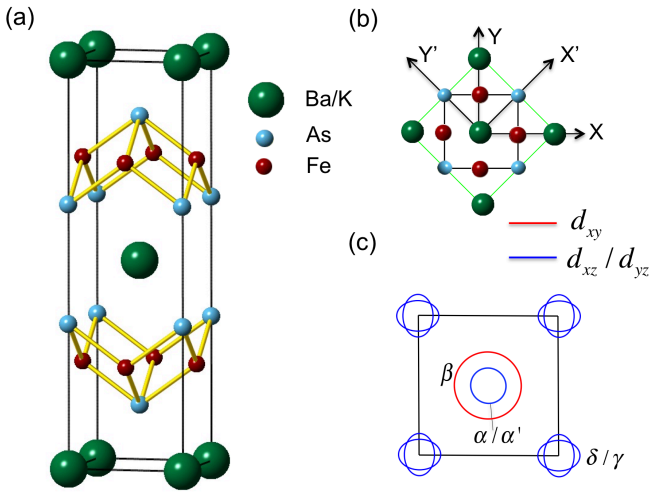

FIG. 1. (Color online) (a) Crystal structure of $Ba_{1-x}K_xFe_2As_2$. (b) Definition of the X, Y, X′ and Y′ directions. The green and black lines represent the 4-Fe and 2-Fe unit cells, respectively. (c) Schematic representation of the Fermi surface of $Ba_{1-x}K_xFe_2As_2$ in the 2-Fe Brillouin zone.

III. RESULTS

A. Normal state

In Figs. 2(a)-2(i), we show the normal state Raman spectra of $Ba_{1-x}K_xFe_2As_2$ in three different symmetry channels. The sharp mode around 182 cm^{-1} detected at room temperature in Figs. 2(a)-2(c) corresponds to a A_{1g} phonon. The phonon frequency hardens upon cooling [38]. The phonon intensity strengthens with K doping. The B_{2g} symmetry electronic continuum strengthens upon cooling from 300 K to 40 K [Figs. 2(d)-2(f)]. In particular, at low temperature a broad low-energy feature centered around 100 cm^{-1} develops. Similar quasi-elastic scattering was previously related to quadrupolar nematic fluctuations [19, 39]. We note that the intensity of this quasi-elastic scattering for $Ba_{1-x}K_xFe_2As_2$ is weaker than for $Ba(Fe_{1-x}Co_x)_2As_2$ [23, 40, 41], which is possibly due to the different anisotropic properties of the electron-doped and hole-doped Fe-based superconductors also noted by resistivity measurements [42, 43]. In addition to the B_{1g} phonon at 208 cm^{-1}, the spectra in the B_{1g} symmetry channel also contains quasi-elastic scattering features similar to the one discussed above [Figs. 2(g)-2(i)].

In Figs. 2(j)-2(l), we show the static Raman susceptibilities $\chi_{B_{1g}}(0,T)$ and $\chi_{B_{2g}}(0,T)$ obtained *via* the Kramers-Kronig transformation with a high-energy cut-

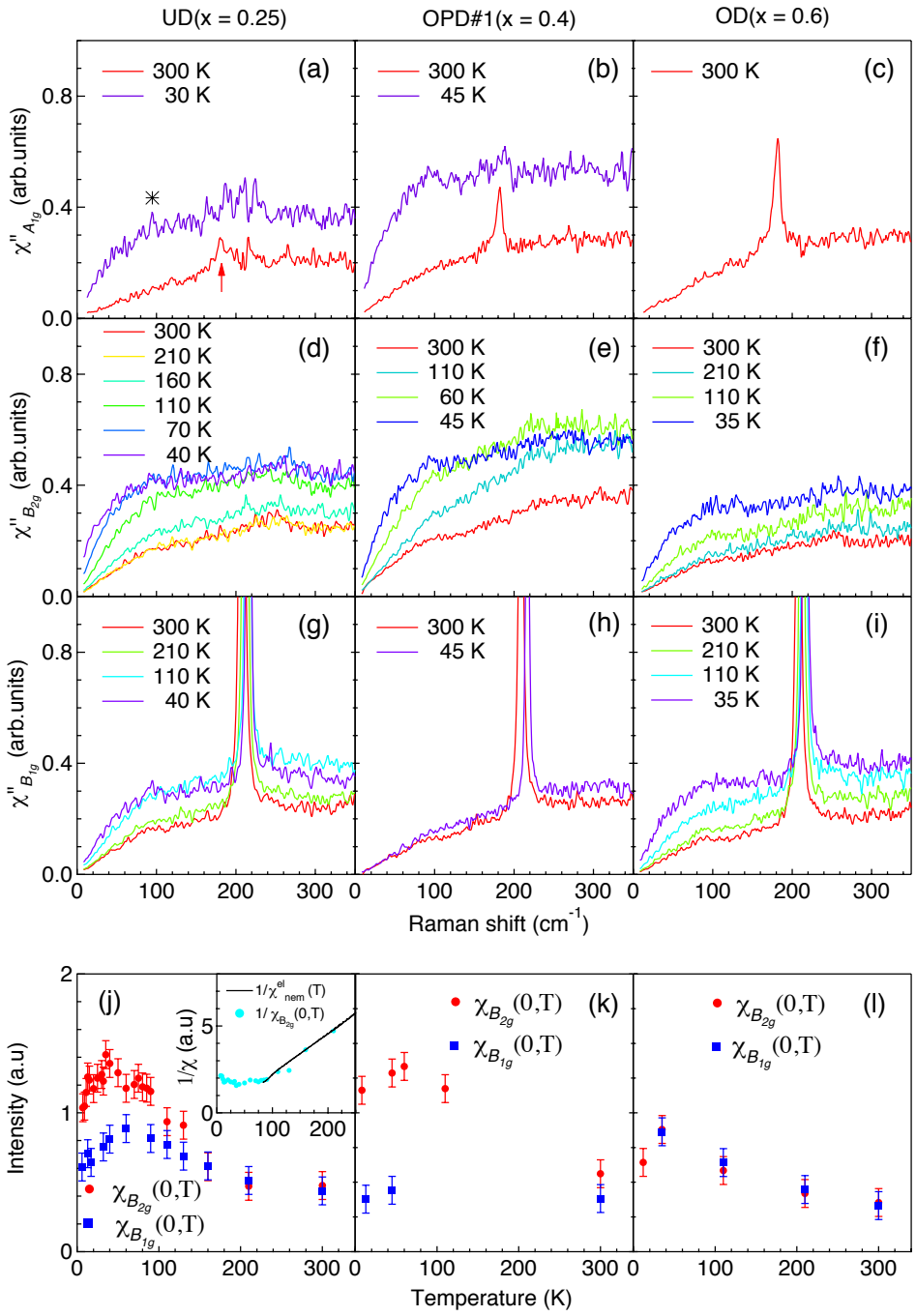

FIG. 2. (Color online). Doping and temperature evolution of the Raman susceptibility of $Ba_{1-x}K_xFe_2As_2$ in different symmetry channels. Left column: UD ($x = 0.25$); Central column: OPD#1($x = 0.4$); Right column: OD ($x = 0.6$). (a)-(c) Temperature dependence of the Raman response in the A_{1g} channel. The asterix in (a) marks a small peak due to laser plasma, whereas the arrow indicates a A_{1g} phonon. (d)-(f) Temperature dependence of the Raman response in the B_{2g} channel. (g)-(i) Same as (d)-(f) but for the B_{1g} channel. (j)-(l) T-dependence of the static Raman susceptibilities $\chi_{B_{2g}}(0,T)$ (red solid circles) and $\chi_{B_{1g}}(0,T)$ (blue solid squares). The inset of (j) shows the inverse nematic susceptibility $1/\chi^{el}_{nem}$ (black line) of $Ba_{0.86}K_{0.24}Fe_2As_2$ extracted from Young's modulus measurements in Ref. [37]. The cyan dots in the inset of (j) are values of $1/\chi_{B_{2g}}(0,T)$ derived from Raman.

off at 350 cm^{-1} justified by an already small $\chi''(\omega)/\omega$ integrand at that energy. We used a linear extrapolation for the $\chi''(\omega)$ below 10 cm^{-1}. The B_{1g} phonon was removed by fitting before the Kramers-Kronig transfor-

mation. The susceptibilities show general enhancement upon cooling from room temperature followed by a mild reduction at low temperatures. $\chi_{B_{2g}}(0,T)$ is larger than $\chi_{B_{1g}}(0,T)$ in the under-doped [Fig. 2 (k)] and optimally-doped [Fig. 2 (l)] samples, suggesting that the B_{2g} channel is the dominant channel for the nematic fluctuations. However, the B_{1g} and B_{2g} symmetry susceptibilities are quite similar in the over-doped regime. In a recent study of $BaFe_2(As_{0.5}P_{0.5})_2$, it was argued that the similarity between the $\chi_{B_{1g}}(0,T)$ and $\chi_{B_{2g}}(0,T)$ static susceptibilities could originate from a disorder due to As/P substitution [44]. The same argument could also apply here due to the Ba/K substitution.

In the inset of Fig. 2(j), we show the inverse of the static susceptibility $1/\chi_{B_{2g}}(0,T)$ and compare it to the measurements of the elastic modulus $C_{66}(T)$ [45]. Following the model proposed in the Ref. [37], $C_{66}(T)$ is renormalized due to the electron-lattice coupling following $C_{66}(T) = C_{66,0}\text{-}\lambda^2\chi_\phi(T)$, where $C_{66,0}$ is the bare elastic constant, ϕ is the nematic order parameter, χ_ϕ is the related nematic susceptibility, λ is the electron-lattice coupling constant [37, 46]. The electronic nematic susceptibility $\chi^{el}_{nem}(T)$ can thus be derived from measurements of the elastic modulus $C_{66}(T)$ [45] (or Young's modulus $Y_{110}(T)$ with $C_{66}/C_{66,0} \approx Y_{110}/Y_0$ [37].) As shown in the inset of Fig. 2(j), $1/\chi_{B_{2g}}(0,T)$ from Raman measurements scales satisfactorily with $1/\chi^{el}(T)$ computed and scaled from Young's modulus measurements of $Ba_{0.86}K_{0.24}Fe_2As_2$ from Ref. [37]. This scaling above T_S in the under-doped regime suggests that the softening of C_{66} [45] and the enhancement of the Raman static susceptibility upon cooling are related.

B. Superconducting state

Before discussing the Raman scattering features observed at low temperature, we recall the SC gap values obtained by complementary spectroscopic probes in optimally-doped $Ba_{1-x}K_xFe_2As_2$. ARPES studies report nodeless SC gaps on all Fermi surface (FS) pockets, with small or negligible in-plane anisotropy [50, 51]. While a SC gap of 6 meV is found on the holelike β (d_{xy}) FS centered at the Γ point, a larger gap of about 12 meV is found on all the other pockets, with differences smaller than a meV [52]. An ARPES study of the SC gap using synchrotron radiation, which allows to vary the k_z position, indicates that the gap size on each FS does not vary significantly with k_z, except for the Γ-centered hole FS formed by the even combination of the d_{xz} and d_{yz} orbitals, for which a gap varies between 9 and 12 meV [56]. Results compatible with ARPES are obtained by STS, which reveals two coherence SC peaks at 10.5 meV and 6 meV [53], and by optical conductivity, for which a SC gap of 12.5 meV opens below T_c [57]. Thermal conductivity measurements are consistent with nodeless gaps for the optimally-doped compound [58]. At the energy scale similar to the SC gaps, a 14 meV neutron resonance mode is reported below T_c at the antiferromagnetic wave-vector **Q** [13]. Interestingly, a 13±2 meV mode energy determined from a kink in the electronic dispersion is observed by ARPES below T_c on bands quasi-nested by the antiferromagnetic wave-vector [15]. STS measurements also reveal coupling to a bosonic mode at 14 meV [16]. We summarize values of the SC gaps and bosonic modes deduced from different spectroscopies in TABLE I.

TABLE I. Summary of the SC gaps and bosonic modes deduced from Raman scattering, ARPES, STS and inelastic neutron scattering (INS). UD, OPD and OD refer to under-doped, optimally-doped and over-doped samples, respectively. We caution that the doping of the under-doped and over-doped samples measured by different techniques may be different and that the collective modes observed by Raman and by other types of spectroscopies may have different origins. All energies are given in units of meV.

	Raman (This work)	Raman ([21, 22])	ARPES	STS	INS
$\Delta_\alpha^{(UD)}$			9 [47]	6 [48]	
$\Delta_\beta^{(UD)}$	3.8		4 [47]	3.8 [48]	
$E_{CM}^{(UD)}$	12			8 [48]	12.5 [49]
$\Delta_\alpha^{(OPD)}$	10.8 (B_{2g})	10.6	9-13 [50–52]	10.5 [53]	
$\Delta_\beta^{(OPD)}$	4.4	4.4	5-6 [50–52]	6 [53]	
$E_{CM}^{(OPD)}$	17.5	17.5	13±2 [15]	14 [16]	14 [13]
$\Delta_\alpha^{(OD)}$	10		8 [54]	6 [53]	
$\Delta_\beta^{(OD)}$	3		4 [54]	3 [53]	
$E_{CM}^{(OD)}$	14				12 [55]

1. *The optimal doping*

In Fig. 3, we compare the Raman spectra at 45 K (normal state) and 6 K (SC state) in three symmetry channels from optimally-doped samples OPD#1 and OPD#2. We first start describing results from the OPD#2 sample. In Fig. 3(a), two broad and weak features emerge around 70 cm^{-1} and 210 cm^{-1}, which we assign to A_{1g} SC pair breaking peaks corresponding to gap values 2Δ of 8.8 meV and 26.2 meV, respectively. In Fig. 3(b), a small spectral weight suppression is seen below 160 cm^{-1} in the B_{1g} channel. In Fig. 3(c), a broad and weak feature at 70 cm^{-1} (8.8 meV) is observed in the B_{2g} channel, which we assign to the small gap $2\Delta_\beta$ on the β FS pocket with d_{xy} character [50, 51]. Another sharp mode at 172 cm^{-1} associated with a SC pair breaking peak at $2\Delta_\alpha = 21.6$ meV appears in the B_{2g} channel, which is consistent with the 10-13 meV magnitude measured by ARPES for the large SC gap around $k_z = 0$ [50–52]. The large gap value varies from 10.8 meV in the B_{2g} channel to 13.1 meV in the A_{1g} channel, in agreement with ARPES measurements revealing an anisotropic gap along k_z [56]. Between $2\Delta_\beta$ and $2\Delta_\alpha$, we detect a sharp mode at $E_{CM} = 140\,cm^{-1}$ (17.5 meV), which will be discussed below.

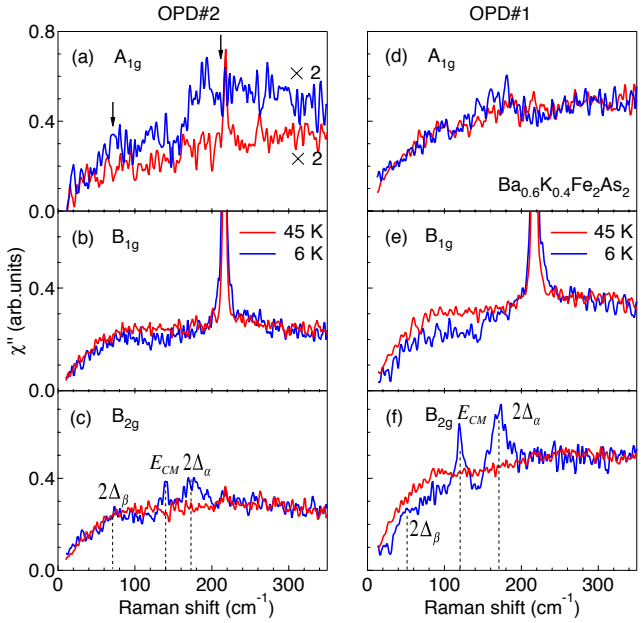

FIG. 3. (Color online) (a)-(c) Raman response of $Ba_{0.4}K_{0.6}Fe_2As_2$ (OPD#2) at 45 K (red) and 6 K (blue) in the (a) A_{1g}, (b) B_{1g}, and (c) B_{2g} channels. The dashed lines in (c) mark a broad feature at 70 cm^{-1} ($2\Delta_\beta$), a collective mode (E_{CM}) around 140 cm^{-1} and a pair-breaking peak at 172 cm^{-1} ($2\Delta_\alpha$). (d)-(f) Same as (a)-(c) but for sample OPD#1. For the OPD#1 sample we find $2\Delta_\beta = 50$ cm^{-1}, $E_{CM} = 120$ cm^{-1} and $2\Delta_\alpha = 168$ cm^{-1}.

For the OPD#1 sample, only a small broad feature around 160 cm^{-1} is seen in the A_{1g} symmetry response [Fig. 3(d)]. In contrast, the spectral features in the B_{1g} and B_{2g} channels appear more clearly for the OPD#1 sample than for the OPD#2 sample. In Fig. 3(e), a spectral weight suppression below T_c is seen below 160 cm^{-1} in the B_{1g} channel. For the B_{2g} channel, two sharp modes at 120 cm^{-1} and 168 cm^{-1}, as well as a kink feature at 50 cm^{-1}, are seen in Fig. 3(f). While little change is observed for the large SC gap pair breaking peak energy as compared to the OPD#2 sample, a substantial shift from 70 cm^{-1} to 50 cm^{-1} is observed for the small SC gap pair breaking peak energy. The sharp E_{CM} mode shifts by the same amount, from 140 cm^{-1} to 120 cm^{-1} in the OPD#1 sample. Since the results for the OPD#2 sample are consistent with previous Raman work [21] for the optimally-doped compound, we caution that the OPD#1 sample cleaved in this study must have a slightly different doping due to inhomogeneous K distribution in the bulk or rapid sample aging.

In addition to the sharp peak, a threshold is also observed around 30 cm^{-1} in the SC state [Figs. 3(e) and 3(f)]. This threshold suggests a fundamental gap of 1.9 meV, consistent with the 2 meV-wide flat bottom in the STS spectra [53]. No clear threshold is detected in the OPD#2 sample though, possibly because the cleaved surface is not good enough, as suggested by weaker peaks

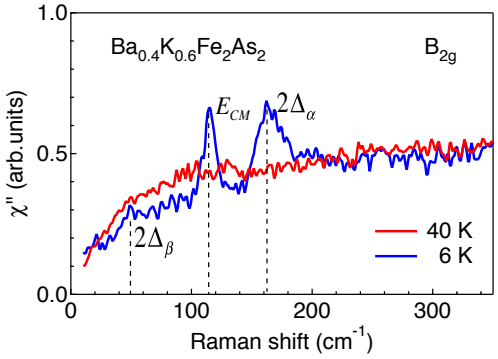

FIG. 4. (Color online) Raman response of $Ba_{0.6}K_{0.4}Fe_2As_2$ (OD) at 40 K (red) and 6 K (blue) in the B_{2g} channel. The dashed lines mark a broad peak at 50 cm^{-1} ($2\Delta_\beta$), a collective mode E_{CM} at 115 cm^{-1} and a pair breaking peak at 162 cm^{-1} ($2\Delta_\alpha$).

in the B_{2g} channel.

2. *The over-doped regime*

We now discuss the spectra from the over-doped sample. In Fig. 4, we compare the Raman response obtained at 40 K (normal state) and 6 K (SC state) in the B_{2g} channel. Four features are clearly observed: a threshold around 30 cm^{-1}, a kink-like feature around 50 cm^{-1}, and two sharp modes at 115 cm^{-1} and 162 cm^{-1}. As with the OPD#1 sample, we assign the threshold to a fundamental SC gap. The kink around 50 cm^{-1} corresponds to the small SC gap pair breaking peak with $2\Delta_\beta = 6$ meV. The sharp mode at 162 cm^{-1} corresponds to the large SC gap pair breaking peak with $2\Delta_\alpha = 20$ meV. As a comparison, an ARPES study on over-doped $Ba_{0.7}K_{0.3}Fe_2As_2$ ($T_c = 22$ K) gives $\Delta_\alpha = 8$ meV and $\Delta_\beta = 4$ meV [54]. Finally, the sharp mode at 115 cm^{-1} (14 meV) is associated to the E_{CM} mode. We note that all the features for the OD sample are similar to those for the OPD#1 sample, confirming that the OPD#1 sample might be slightly over-doped.

3. *The under-doped regime*

We now discuss results for the under-doped regime. In the left column of Fig. 5, we compare the Raman responses $\chi''(\omega)$ from the under-doped sample at 40 K (normal state) and 6 K (SC state) in three symmetry channels. A small suppression of spectral weight is observed below T_c at low energies in the A_{1g} channel [Fig. 5(a)], and the spectra barely change in the B_{1g} channel [Fig. 5(b)]. In the B_{2g} channel, however, spectral weight is transferred from the low-energy, and a sharp peak at 60 cm^{-1} builds up. This peak is also seen when 752 nm excitation is used, as shown in the inset

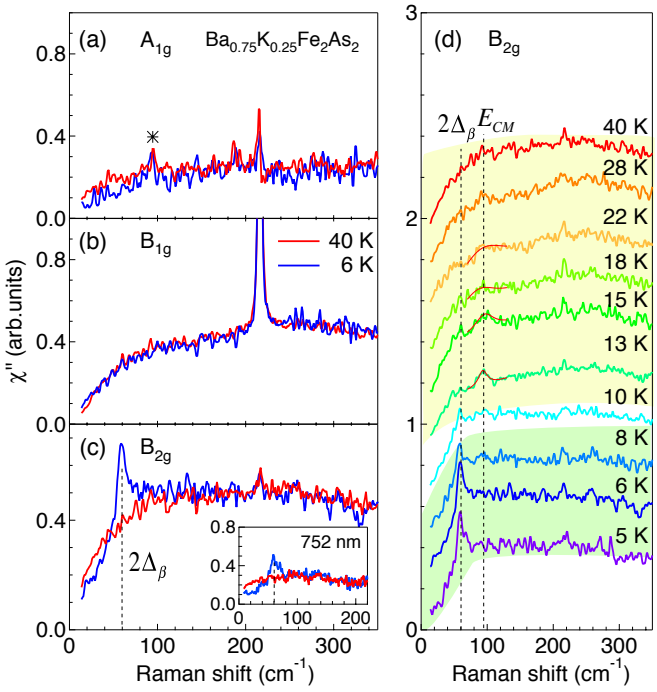

FIG. 5. (Color online). Raman response of $Ba_{0.75}K_{0.25}Fe_2As_2$ (UD30K) at 40 K (red) and 6 K (blue) for the (a) A_{1g}, (b) B_{1g}, and (c) B_{2g} symmetries. The star in (a) represents a laser plasma line. The inset in (c) shows the Raman responses recorded with a 752 nm laser excitation. (d) $\chi''_{B_{2g}}(\omega)$ at various temperatures. The dashed lines in (d) indicate $2\Delta_\beta$ and E_{CM}. The red curves in (d) are fits of the E_{CM} peaks. The yellow and green shadings emphasize different spectral backgrounds associated to different phases.

of Fig. 5(c). Following the interpretation of the kink observed at 70 cm^{-1} at optimal doping, we attribute the 60 cm^{-1} feature in the UD sample to a pair breaking peak with $2\Delta_\beta = 7.5$ meV, which is consistent with the $\Delta_\beta = 4$ meV gap value reported by ARPES measurements for the β (d_{xy}) Γ-centered hole FS pocket for samples with similar doping level [47]. Surprisingly, the sharp SC pair breaking peak at 172 cm^{-1} observed at low temperature for optimally-doped samples is absent in the UD sample. Although the reason for this disappearance is unclear, we caution that it may be related to the loss of coherence observed by ARPES experiments for the d_{xz}/d_{yz} bands [47].

As illustrated by the fine temperature dependence of the B_{2g} Raman response in Fig. 5(d), the sharp peak at 60 cm^{-1} appears clearly only below 10 K. Interestingly, the B_{2g} spectrum exhibits clear changes across that temperature, as highlighted with yellow and green backgrounds in Fig. 5(d). For example, below 10 K the spectral background is flat between 100 cm^{-1} and 350 cm^{-1}, but shows a broad feature above that temperature. These observations are consistent with recent studies on $Ba_{1-x}K_xFe_2As_2$ [59, 60] and $Ba_{1-x}Na_xFe_2As_2$ [61, 62] suggesting re-entrance into the C_4 preserved magnetic phase in the under-doped regime. Within this context, the broad feature above 10 K can be interpreted as the formation of a spin-density-wave gap below the magnetic phase transition. We note that a pseudo-gap of about 17 meV was observed by ARPES below 125 K in under-doped $Ba_{0.75}K_{0.25}Fe_2As_2$ [47]. Assuming that this pseudo-gap is approximately symmetric with respect to the Fermi energy, it would lead to a Raman feature at twice this value ($\sim$ 35 meV), which is roughly the position of the broad feature observed in Raman data. The sudden disappearance of the broad feature below 10 K could be explained either by a non-magnetic low-temperature phase ($T < 10$ K), which would contradict the phase diagram presented in Ref. [59], by a different magnetic structure, or by restoring the four-fold symmetry at the lowest temperature. The E_{CM} mode in the UD sample is detected around 95 cm^{-1} only between 22 K and 13 K, emphasizing further the difference between the phases above and below the phase transition at 10 K.

TABLE II. Summary of the binding energy of the in-gap mode in the B_{2g} channel for the OPD and OD samples. All values are given in cm^{-1}.

Sample	$2\Delta_\alpha$	E_{CM}	E_B	$E_B/2\Delta_\alpha$
OPD#2	172	140	32	0.2
OD	162	115	47	0.3

IV. DISCUSSION

In this section we discuss the origin of the E_{CM} mode. In Fig. 6(b), we plot the doping dependence of the difference between the B_{2g} Raman response function recorded in the SC state at 6 K, deep in the SC state, and at the normal state. Although both the $2\Delta_\alpha$ and $2\Delta_\beta$ peaks shift with doping, the shift is more pronounced for the later one [see Fig. 6(c)]. Interestingly, the E_{CM} mode moves almost by the same amount as the $2\Delta_\beta$ peak: the mode is observed at 95 cm^{-1} (11.9 meV) for $x = 0.25$, at 140 cm^{-1} (17.5 meV) in for $x = 0.4$ and at 115 cm^{-1} (14.4 meV) for $x = 0.6$ doping levels. The E_{CM} mode energy is higher than the gap typically observed by ARPES for the β (d_{xy}) band and smaller than the gap observed on the other FSs for corresponding dopings [47, 50, 51]. Consequently, the E_{CM} mode is unlikely related to a SC pair breaking peak on the same band.

We note that the E_{CM} mode energy is similar to the sum $\Delta_\beta + \Delta_\alpha$. One speculative explanation for the E_{CM} related to an inter-band scattering process lies in the observation of in-gap impurity states by ARPES below T_c [63]: a photon breaks a Cooper pair out of the condensate and creates a quasi-particle on the band with an energy cost Δ_α, while the second particle from the broken pair is scattered into a quasi-particle state of the band with the smaller gap (energy cost Δ_β), with the help of an impurity taking the recoil for conservation of

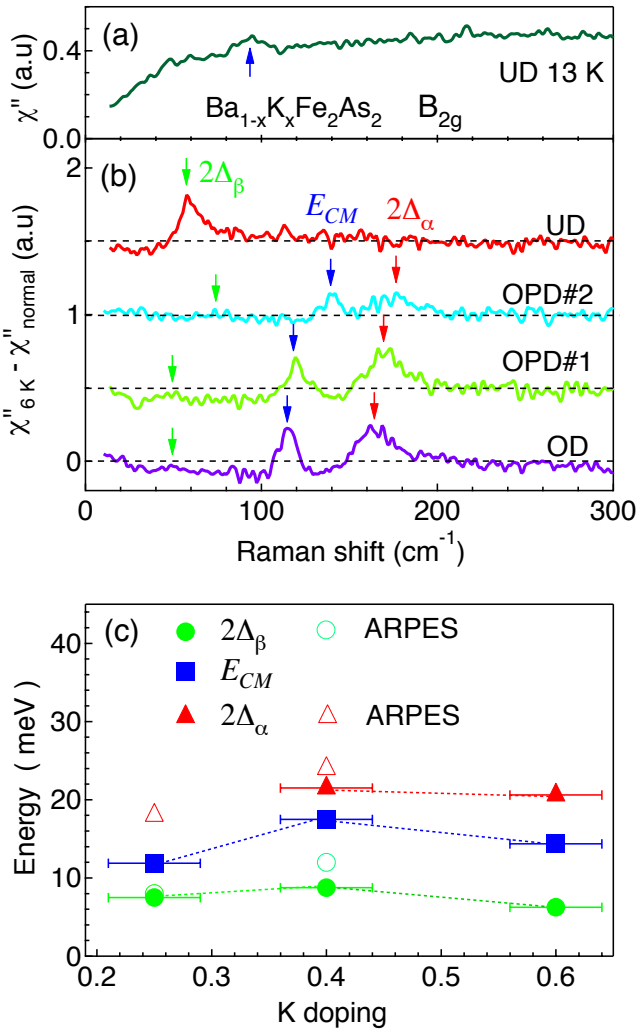

FIG. 6. (Color online). (a) Raman response of $Ba_{0.75}K_{0.25}Fe_2As_2$ in the B_{2g} channel at 13 K. (b) Difference between the Raman spectra at 6 K in the SC state and in the normal state, recorded in the B_{2g} channel for different dopings. (c) Summary of the SC pair breaking peaks and in-gap mode in $Ba_{1-x}K_xFe_2As_2$ obtained in the B_{2g} channel. The full and open symbols correspond to results from this work and from ARPES [47, 50, 51], respectively.

the quasi-momentum. Due to the residual interaction coming from both pairing and Coulomb interaction between two quasi-particles on different bands, and to some charge transfer between bands, the cost of this process is slightly smaller than $\Delta_\alpha+\Delta_\beta$. However, it is not clear within this scenario why the related Raman mode is so sharp and symmetric.

We note that the energy of the E_{CM} mode is similar to that of the neutron resonance mode observed only below T_c in the triplet channel at the antiferromagnetic wave vector [13] and to the kink energy observed in the quasi-particle dispersion by ARPES also only below T_c [15]. In principle, only spin singlet modes with nearly zero momentum transfer can be probed by Raman scattering. Thus, the neutron resonance mode and the Raman collective mode are distinct. The fact that the binding energies of these two modes are similar suggests that the interaction leading to the origin of in-gap resonance in the magnetic channel is not that different from the attraction in the spin singlet channel. In other words, interactions at momentum transfer $\mathbf{q} = 0$ and $\mathbf{q} = \mathbf{Q}$ (such as intra-pocket and inter-pocket interactions, respectively), have similar strength. Hence, a proper model description of the collective modes in such superconductor, must consider both types of interactions on equal footing.

In Table II, we summarize the binding energy $E_B = 2\Delta_\alpha - E_{CM}$ and the ratio between the binding energy and the large gap edge $E_B/2\Delta_\alpha$ for OPD#2 and OD samples. With doping the binding energy increases from 32 cm^{-1} for optimally-doped regime to 47 cm^{-1} for the over-doped regime, and the ratio $E_B/2\Delta_\alpha$ increases from 0.2 to 0.3, indicating enhancement of the residual interactions with doping.

The interaction could originate from the attraction in sub-dominant symmetry particle-particle channel leading to a Bardasis-Schrieffer (BS) like exciton [19, 24, 26, 29, 31, 33] or, alternatively, from particle-hole attraction leading to nematic fluctuations and a Pomeranchuk-like exciton [19, 20, 27, 33, 34]. The increase of the binding energy with doping within the first BS scenario is an indication that the competing d-wave symmetry interaction strengthen with doping. Indeed, although fully gapped superconductivity is well established in the optimally doped regime, numerous experiments suggest that transition from nodeless to nodal order parameter appear in the heavily hole-doped regime for $x > 0.8$ [64–68]. Because the structural instability is suppressed with K-doping, the nematic interactions weaken, in agreement with the observed reduction of the nematic susceptibility with doping [Fig. 2 (j-l)].

However, the nematic fluctuations can grow stronger below T_c, where low-lying excitations are gapped and thus the damping of the nematic fluctuations is removed. In this case nematic fluctuations can gain coherence and lead to a particle-hole exciton mode manifesting itself as a sharp resonance in the B_{2g} channel [19, 20, 34]. Interestingly, the collective modes that appear in the tetragonal phase of the optimally-doped and over-doped samples are sharper and stronger than that in the orthorhombic phase of the under-doped regime, likely due to suppressed nematic fluctuations in the orthorhombic phase, where the four-fold symmetry is broken.

We note that for a multi-band system the interactions of the particle-particle and particle-hole channels of the same symmetry representation mix. Therefore, the separation between Bardasis-Schrieffer-like and Pomeranchuk-like excitons is artificial as both the particle-particle and particle-hole interactions contribute to formation of the in-gap exciton [33]. We also note that recent theoretical studies show that nematic fluctuations can enhance the s-wave Cooper pairing and thus explain

the enhancement of T_c near the nematic quantum critical point [69, 70].

V. CONCLUSIONS

In conclusion, we used polarization-resolved electronic Raman spectroscopy to probe the electronic properties of $Ba_{1-x}K_xFe_2As_2$ in the normal and SC states as a function of doping ($0.25 \leq x \leq 0.6$). We find that temperature dependent quadrupolar nematic fluctuations are universally present for all studied doping range. The derived dynamic response static Raman susceptibility $\chi_{B_{2g}}(0,T)$ is larger than $\chi_{B_{1g}}(0,T)$, suggesting that nematic fluctuations of the XY symmetry dominate. In particular, the temperature dependence of the static Raman susceptibility $\chi_{B_{2g}}(0,T)$ in the under-doped sample is consistent with measurements of the elastic modulus $C_{66}(T)$, suggesting that the XY-symmetry electronic fluctuations and the lattice are strongly coupled.

In the SC state, for the optimally doped regime, we detected three features in the B_{2g} symmetry Raman response: two pair breaking peaks at 70 cm^{-1} (8.75 meV) and 172 cm^{-1} (21.5 meV) corresponding to a small and a large gap, and an in-gap collective mode at 140 cm^{-1} (17.5 meV). For the over-doped regime, similar three features in B_{2g} channel were observed: two pair breaking peaks at 50 cm^{-1} (6.25 meV) and 115 cm^{-1}(14.38 meV), and an in-gap mode at 162 cm^{-1} (20.25 meV). We discuss scenarios for the origin of the in-gap modes including the mixture of Bardasis-Schrieffer-like and Pomeranchuk-like excitons. The binding energy of the in-gap mode increases from optimal doping to over-doping, suggesting a possible transition from nodeless $s_{\pm}$ order parameter to a nodal d-wave order parameter at higher K doping concentration.

In the under-doped regime, the B_{2g} symmetry pair breaking peak corresponding to the large gap is undetectable. We detected a sharp pair breaking peak at 60 cm^{-1} (3.8 meV) corresponding to the small gap. In addition, the shape of the spectral background changes at 10 K, suggesting two distinct SC phases in the under-doped regime. We observed a broader peak at 95 cm^{-1} above 10 K, which we assign to the collective in-gap mode in the under-doped regime.

ACKNOWLEDGMENTS

We acknowledge useful discussions with K. Haule, V. K. Thorsmølle, W.-L. Zhang, P. Zhang, H. Miao, and J.-X.Yin. We acknowledge H.-H. Kung and B. Dennis for help with the experiments. The spectroscopic study and analysis at Rutgers were supported by the US Department of Energy, Basic Energy Sciences, and Division of Materials Sciences and Engineering under Grant No. DE-SC0005463. The materials characterization at IOP, was supported by grants from MOST (2015CB921301, 2016YFA0401000, 2016YFA0300300) and NSFC (11274362, 11674371) of China. The crystal growth was supported by grants from MOST(2011CBA00102) and NSFC(11534005) of China.

[1] I. I. Mazin and J. Schmalian, "Pairing symmetry and pairing state in ferropnictides: Theoretical overview," Physica C **469**, 614 (2009).
[2] S. Graser, T. A. Maier, P. J. Hirschfeld, and D. J. Scalapino, "Near-degeneracy of several pairing channels in multiorbital models for the Fe pnictides," New J. Phys. **11**, 025016 (2009).
[3] R. M. Fernandes and A. V. Chubukov, "Low-energy microscopic models for iron-based superconductors: a review," Rep. Prog. Phys. **80**, 014503 (2017).
[4] J. Rossat-Mignod, L. P. Regnault, C. Vettier, P. Bourges, P. Burlet, J. Bossy, J. Y. Henry, and G. Lapertot, "Neutron scattering study of the $YBa_2Cu_3O_{6+x}$ system," Physica C **185**, 86 (1991).
[5] H. A. Mook, M. Yethiraj, G. Aeppli, T. E. Mason, and T. Armstrong, "Polarized neutron determination of the magnetic excitations in $YBa_2Cu_3O_7$," Phys. Rev. Lett. **70**, 3490 (1993).
[6] H. F. Fong, P. Bourges, Y. Sidis, L. P. Regnault, A. Ivanov, G. D. Gu, N. Koshizuka, and B. Keimer, "Neutron scattering from magnetic excitations in $Bi_2Sr_2CaCu_2O_{8+\delta}$," Nature **398**, 588 (1999).
[7] P. C. Dai, H. A. Mook, G. Aeppli, S. M. Hayden, and F. Dogan, "Resonance as a measure of pairing correlations in the high-T_c superconductor $YBa_2Cu_3O_{6.6}$," Nature **406**, 965 (2000).
[8] H. He, P. Bourges, Y. Sidis, C. Ulrich, L. P. Regnault, S. Pailhès, N. S. Berzigiarova, N. N. Kolesnikov, and B. Keimer, "Magnetic resonant mode in the single-layer high-temperature superconductor $Tl_2Ba_2CuO_{6+\delta}$," Science **295**, 1045 (2002).
[9] M. Eschrig, "The effect of collective spin-1 excitations on electronic spectra in high-T_c superconductors," Adv. Phys. **55**, 47–183 (2006).
[10] J. Zhao, P. C. Dai, S. L. Li, P. G. Freeman, Y. Onose, and Y. Tokura, "Neutron-spin resonance in the optimally electron-doped superconductor $Nd_{1.85}Ce_{0.15}CuO_{4-\delta}$," Phys. Rev. Lett. **99**, 017001 (2007).
[11] H. F. Fong, B. Keimer, P. W. Anderson, D. Reznik, F. Doğan, and I. A. Aksay, "Phonon and magnetic neutron scattering at 41 meV in $YBa_2Cu_3O_7$," Phys. Rev. Lett. **75**, 316 (1995).
[12] G. Blumberg, Branko P. Stojković, and M. V. Klein, "Antiferromagnetic excitations and van Hove singularities in $YBa_2Cu_3O_{6+x}$," Phys. Rev. B **52**, R15741 (1995).
[13] A. D. Christianson, E. A. Goremychkin, R. Osborn, S. Rosenkranz, M. D. Lumsden, C. D. Malliakas, I. S. Todorov, H. Claus, D. Y. Chung, M. G. Kanatzidis, R. I. Bewley, and T. Guidi, "Unconventional superconductivity in $Ba_{0.6}K_{0.4}Fe_2As_2$ from inelastic neutron scatter-

ing," Nature **456**, 930 (2008).
[14] C. L. Zhang, M. Wang, H. Q. Luo, M. Y. Wang, M. S. Liu, J. Zhao, D. L. Abernathy, T. A. Maier, K. Marty, M. D. Lumsden, S. X Chi, S. Chang, J. A. Rodriguez-Rivera, J. W. Lynn, T. Xiang, J. P. Hu, and P. C. Dai, "Neutron scattering studies of spin excitations in hole-doped $Ba_{0.67}K_{0.33}Fe_2As_2$ superconductor," Sci. Rep. **1**, 115 (2011).
[15] P. Richard, T. Sato, K. Nakayama, S. Souma, T. Takahashi, Y. M. Xu, G. F. Chen, J. L. Luo, N. L. Wang, and H. Ding, "Angle-resolved photoemission spectroscopy of the Fe-Based $Ba_{0.6}K_{0.4}Fe_2As_2$ high temperature superconductor: Evidence for an orbital selective electron-mode coupling," Phys. Rev. Lett. **102**, 047003 (2009).
[16] L. Shan, J. Gong, Y. L. Wang, B. Shen, X. Y. Hou, C. Ren, C.H Li, H. Yang, H. H. Wen, S. L. Li, and P. C Dai, "Evidence of a spin resonance mode in the iron-based superconductor $Ba_{0.6}K_{0.4}Fe_2As_2$ from scanning tunneling spectroscopy," Phys. Rev. Lett. **108**, 227002 (2012).
[17] D. Wu, N. Barišić, M. Dressel, G. H. Cao, Z-A. Xu, E. Schachinger, and J. P. Carbotte, "Eliashberg analysis of optical spectra reveals a strong coupling of charge carriers to spin fluctuations in doped iron-pnictide $BaFe_2As_2$ superconductors," Phys. Rev. B **82**, 144519 (2010).
[18] R. M. Fernandes, A. V. Chubukov, and J. Schmalian, "What drives nematic order in iron-based superconductors?" Nature Phys. **10**, 97 (2014).
[19] V. K. Thorsmølle, M. Khodas, Z. P. Yin, C. L. Zhang, S. V. Carr, P. C Dai, and G. Blumberg, "Critical quadrupole fluctuations and collective modes in iron pnictide superconductors," Phys. Rev. B **93**, 054515 (2016).
[20] Y. Gallais, I. Paul, L. Chauviere, and J. Schmalian, "Nematic resonance in the Raman response of iron-based superconductors," Phys. Rev. Lett. **116**, 017001 (2016).
[21] F. Kretzschmar, B. Muschler, T. Böhm, A. Baum, R. Hackl, H. H Wen, V. Tsurkan, J. Deisenhofer, and A. Loidl, "Raman-scattering detection of nearly degenerate s-wave and d-wave pairing channels in iron-based $Ba_{0.6}K_{0.4}Fe_2As_2$ and $Rb_{0.8}Fe_{1.6}Se_2$ superconductors," Phys. Rev. Lett. **110**, 187002 (2013).
[22] T. Böhm, A. F. Kemper, B. Moritz, F. Kretzschmar, B. Muschler, H.-M. Eiter, R. Hackl, T. P. Devereaux, D. J. Scalapino, and H. H Wen, "Balancing act: Evidence for a strong subdominant d-wave pairing channel in $Ba_{0.6}K_{0.4}Fe_2As_2$," Phys. Rev. X **4**, 041046 (2014).
[23] T. Böhm, R. Hosseinian Ahangharnejhad, D. Jost, A. Baum, B. Muschler, F. Kretzschmar, P. Adelmann, T. Wolf, H. H. Wen, J. H. Chu, I. R. Fisher, and R. Hackl, "Superconductivity and fluctuations in $Ba_{1-p}K_pFe_2As_2$ and $Ba(Fe_{1-n}Co_n)_2As_2$," Phys. Status Solidi B , DOI 10.1002/pssb.201600308 (2016).
[24] A. Bardasis and J. R. Schrieffer, "Excitons and plasmons in superconductors," Phys. Rev. **121**, 1050 (1961).
[25] T. Tsuneto, "Transverse collective excitations in superconductors and electromagnetic absorption," Phys. Rev. **118**, 1029 (1960).
[26] M. V. Klein and S. B. Dierker, "Theory of Raman scattering in superconductors," Phys. Rev. B **29**, 4976 (1984).
[27] M. V. Klein, "Theory of Raman scattering from Leggett's collective mode in a multiband superconductor: Application to MgB_2," Phys. Rev. B **82**, 014507 (2010).
[28] W. C. Lee, S. C. Zhang, and C. J. Wu, "Pairing state with a time-reversal symmetry breaking in FeAs-based superconductors," Phys. Rev. Lett. **102**, 217002 (2009).
[29] S. Maiti and P. J. Hirschfeld, "Collective modes in superconductors with competing s- and d-wave interactions," Phys. Rev. B **92**, 094506 (2015).
[30] D. J. Scalapino and T. P. Devereaux, "Collective d-wave exciton modes in the calculated raman spectrum of fe-based superconductors," Phys. Rev. B **80**, 140512 (2009).
[31] S. Maiti, T.A. Maier, T. Boehm, R. Hackl, and P. J. Hirschfeld, "Probing the pairing interaction and multiple Bardasis-Schrieffer modes using Raman spectroscopy," arXiv:1611.04541 (2016).
[32] A. V. Chubukov, I. Eremin, and M. M. Korshunov, "Theory of Raman response of a superconductor with extended s-wave symmetry: Application to the iron pnictides," Phys. Rev. B **79**, 220501 (2009).
[33] M. Khodas, A. V. Chubukov, and G. Blumberg, "Collective modes in multiband superconductors: Raman scattering in iron selenides," Phys. Rev. B **89**, 245134 (2014).
[34] A Hinojosa, J. S Cai, and A. V. Chubukov, "Raman resonance in iron-based superconductors: The magnetic scenario," Phys. Rev. B **93**, 075106 (2016).
[35] B. Shen, H. Yang, Z. S. Wang, F. Han, B. Zeng, L. Shan, C. Ren, and H. H. Wen, "Transport properties and asymmetric scattering in $Ba_{1-x}K_xFe_2As_2$ single crystals," Phys. Rev. B **84**, 184512 (2011).
[36] T. P. Devereaux and R. Hackl, "Inelastic light scattering from correlated electrons," Rev. Mod. Phys. **79**, 175 (2007).
[37] A. E. Böhmer, P. Burger, F. Hardy, T. Wolf, P. Schweiss, R. Fromknecht, M. Reinecker, W. Schranz, and C. Meingast, "Nematic susceptibility of hole-doped and electron-doped $BaFe_2As_2$ iron-based superconductors from shear modulus measurements," Phys. Rev. Lett. **112**, 047001 (2014).
[38] M. Rahlenbeck, G. L. Sun, D. L. Sun, C. T. Lin, B. Keimer, and C. Ulrich, "Phonon anomalies in pure and underdoped $R_{1-x}K_xFe_2As_2$ (R=Ba, Sr) investigated by Raman light scattering," Phys. Rev. B **80**, 064509 (2009).
[39] W. L. Zhang, P. Richard, H. Ding, A. S. Sefat, J. Gillett, S. E. Sebastian, M. Khodas, and G. Blumberg, "On the origin of the electronic anisotropy in iron pnicitde superconductors," arXiv:1410.6452 (2014).
[40] Y. Gallais, R. M. Fernandes, I. Paul, L. Chauvière, Y. X. Yang, M. A. Méasson, M. Cazayous, A. Sacuto, D. Colson, and A. Forget, "Observation of incipient charge nematicity in $Ba(Fe_{1-x}Co_x)_2As_2$," Phys. Rev. Lett. **111**, 267001 (2013).
[41] F. Kretzschmar, T. Bohm, U. Karahasanovic, B. Muschler, A. Baum, D. Jost, J. Schmalian, S. Caprara, M. Grilli, C. Di Castro, J. G. Analytis, J. H. Chu, I. R. Fisher, and R. Hackl, "Critical spin fluctuations and the origin of nematic order in $Ba(Fe_{1-x}Co_x)_2As_2$," Nature Phys. **12**, 560 (2016).
[42] J. J. Ying, X. F. Wang, T. Wu, Z. J. Xiang, R. H. Liu, Y. J. Yan, A. F. Wang, M. Zhang, G. J. Ye, P. Cheng, J. P. Hu, and X. H. Chen, "Measurements of the anisotropic in-plane resistivity of underdoped FeAs-based pnictide superconductors," Phys. Rev. Lett. **107**, 067001 (2011).
[43] E. C. Blomberg, M. A. Tanatar, R. M. Fernandes, I. I. Mazin, B. Shen, H. H. Wen, M. D. Johannes,

J. Schmalian, and R Prozorov, "Sign-reversal of the in-plane resistivity anisotropy in hole-doped iron pnictides," Nat. Commun. **4**, 1914 (2013).

[44] S. F. Wu, W. L. Zhang, D. Hu, H. H Kung, A. Lee, H. C. Mao, P. C. Dai, H. Ding, P. Richard, and G. Blumberg, "Collective excitations of dynamic Fermi surface deformations in $BaFe_2(As_{0.5}P_{0.5})_2$," arXiv:1607.06575 (2016).

[45] T. Goto, R. Kurihara, K. Araki, K. Mitsumoto, M. Akatsu, Y. Nemoto, S. Tatematsu, and M. Sato, "Quadrupole effects of layered iron pnictide superconductor $Ba(Fe_{0.9}Co_{0.1})_2As_2$," J. Phys. Soc. Jpn. **80**, 073702 (2011).

[46] R. M. Fernandes, L. H. VanBebber, S. Bhattacharya, P. Chandra, V. Keppens, D. Mandrus, M. A. McGuire, B. C. Sales, A. S. Sefat, and J. Schmalian, "Effects of nematic fluctuations on the elastic properties of iron arsenide superconductors," Phys. Rev. Lett. **105**, 157003 (2010).

[47] Y. M. Xu, P. Richard, K. Nakayama, T. Kawahara, Y. Sekiba, T. Qian, M. Neupane, S. Souma, T. Sato, T. Takahashi, H. Q. Luo, H. H. Wen, G. F. Chen, N. L. Wang, Z. Wang, Z. Fang, X. Dai, and H. Ding, "Fermi surface dichotomy of the superconducting gap and pseudogap in underdoped pnictides," Nat. Commun. **2**, 394 (2011).

[48] J. Gong, X. Y. Hou, J. Zhu, Y. Y. Jie, Y. D. Gu, B. Shen, C. Ren, C. H. Li, and L. Shan, "Observation of mode-like features in tunneling spectra of iron-based superconductors," Chin. Phys. B **24**, 077402 (2015).

[49] J. P. Castellan, S. Rosenkranz, E. A. Goremychkin, D. Y. Chung, I. S. Todorov, M. G. Kanatzidis, I. Eremin, J. Knolle, A. V. Chubukov, S. Maiti, M. R. Norman, F. Weber, H. Claus, T. Guidi, R. I. Bewley, and R. Osborn, "Effect of Fermi surface nesting on resonant spin excitations in $Ba_{1-x}K_xFe_2As_2$," Phys. Rev. Lett. **107**, 177003 (2011).

[50] H. Ding, P. Richard, K. Nakayama, K. Sugawara, T. Arakane, Y. Sekiba, A. Takayama, S. Souma, T. Sato, T. Takahashi, Z. Wang, X. Dai, Z. Fang, G. F. Chen, J. L. Luo, and N. L. Wang, "Observation of Fermi-surface-dependent nodeless superconducting gaps in $Ba_{0.6}K_{0.4}Fe_2As_2$," Europhys. Lett. **83**, 47001 (2008).

[51] L. Zhao, H. Y. Liu, W. T. Zhang, J. Q. Meng, X. W. Jia, G. D. Liu, X. L Dong, G. F. Chen, J. L. Luo, N. L. Wang, W. Lu, G. L. Wang, Y. Zhou, Y. Zhu, X. Y. Wang, Z. Y Xu, C. T. Chen, and X. J. Zhou, "Multiple nodeless superconducting gaps in $Ba_{0.6}K_{0.4}Fe_2As_2$ superconductor from angle-resolved photoemission spectroscopy," Chin. Phys. Lett. **25**, 4402 (2008).

[52] K. Nakayama, T. Sato, P. Richard, Y. M. Xu, Y. Sekiba, S. Souma, G. F. Chen, J. L. Luo, N. L. Wang, H. Ding, and T. Takahashi, "Superconducting gap symmetry of $Ba_{0.6}K_{0.4}Fe_2As_2$ studied by angle-resolved photoemission spectroscopy," Europhys. Lett. **85**, 67002 (2009).

[53] J. X. Yin, A. Li, X. X. Wu, J. Li, Z. Wu, J. H. Wang, C. S. Ting, P. H. Hor, X. J. Liang, C. L. Zhang, P. C. Dai, X. C. Wang, C. Q. Jin, G. F. Chen, J. P. Hu, Z. Q. Wang, and S. H. Pan, "Real-space orbital-selective probing of the cooper pairing in iron pnictides," arXiv:1602.04949 (2016).

[54] K. Nakayama, T. Sato, P. Richard, Y. M. Xu, T. Kawahara, K. Umezawa, T. Qian, M. Neupane, G. F. Chen, H. Ding, and T. Takahashi, "Universality of superconducting gaps in overdoped $Ba_{0.3}K_{0.7}Fe_2As_2$ observed by angle-resolved photoemission spectroscopy," Phys. Rev. B **83**, 020501 (2011).

[55] C. H. Lee, K. Kihou, J. T. Park, K. Horigane, K. Fujita, F. Waßer, N. Qureshi, Y. Sidis, J. Akimitsu, and M. Braden, "Suppression of spin-exciton state in hole overdoped iron-based superconductors," Sci. Rep. **6**, 23424 (2016).

[56] Y. M. Xu, Y. B. Huang, X. Y. Cui, E. Razzoli, M. Radovic, M. Shi, G. F. Chen, P. Zheng, N. L. Wang, C. L. Zhang, P. C. Dai, J. P. Hu, Z. Wang, and H. Ding, "Observation of a ubiquitous three-dimensional superconducting gap function in optimally doped $Ba_{0.6}K_{0.4}Fe_2As_2$," Nature Phys. **7**, 198 (2011).

[57] G. Li, W. Z. Hu, J. Dong, Z. Li, P. Zheng, G. F. Chen, J. L. Luo, and N. L. Wang, "Probing the superconducting energy gap from infrared spectroscopy on a $Ba_{0.6}K_{0.4}Fe_2As_2$ single crystal with $T_c = 37$ K," Phys. Rev. Lett. **101**, 107004 (2008).

[58] X. G. Luo, M. A. Tanatar, J. P. Reid, H. Shakeripour, N. Doiron-Leyraud, N. Ni, S. L. Bud'ko, P. C. Canfield, H. Q Luo, Z. S Wang, H. H Wen, R. Prozorov, and L. Taillefer, "Quasiparticle heat transport in single-crystalline $Ba_{1-x}K_xFe_2As_2$: Evidence for a k-dependent superconducting gap without nodes," Phys. Rev. B **80**, 140503 (2009).

[59] A. E. Böhmer, F. Hardy, L. Wang, T. Wolf, P. Schweiss, and C. Meingast, "Superconductivity-induced re-entrance of the orthorhombic distortion in $Ba_{1-x}K_xFe_2As_2$," Nat. Commun. **6** (2015).

[60] J. M. Allred, S. Avci, D. Y. Chung, H. Claus, D. D. Khalyavin, P. Manuel, K. M. Taddei, M. G. Kanatzidis, S. Rosenkranz, R. Osborn, and O. Chmaissem, "Tetragonal magnetic phase in $Ba_{1-x}K_xFe_2As_2$ from x-ray and neutron diffraction," Phys. Rev. B **92**, 094515 (2015).

[61] D. D. Khalyavin, S. W. Lovesey, P. Manuel, F. Krüger, S. Rosenkranz, J. M. Allred, O. Chmaissem, and R. Osborn, "Symmetry of reentrant tetragonal phase in $Ba_{1-x}Na_xFe_2As_2$: Magnetic versus orbital ordering mechanism," Phys. Rev. B **90**, 174511 (2014).

[62] L. Wang, F. Hardy, A. E. Böhmer, T. Wolf, P. Schweiss, and C. Meingast, "Complex phase diagram of $Ba_{1-x}Na_xFe_2As_2$: A multitude of phases striving for the electronic entropy," Phys. Rev. B **93**, 014514 (2016).

[63] P. Zhang, P. Richard, T. Qian, X. Shi, J. Ma, L. K. Zeng, X. P. Wang, E. Rienks, C. L. Zhang, P. C Dai, Y. Z. You, Z. Y. Weng, X. X. Wu, J. P. Hu, and H. Ding, "Observation of momentum-confined in-gap impurity state in $Ba_{0.6}K_{0.4}Fe_2As_2$: Evidence for antiphase $s_\pm$ pairing," Phys. Rev. X **4**, 031001 (2014).

[64] T. Shibauchi, A. Carrington, and Y. Matsuda, "A quantum critical point lying beneath the superconducting dome in iron pnictides," Annu. Rev. Condens. Matter Phys. **5**, 113 (2014).

[65] H. Fukazawa, Y. Yamada, K. Kondo, T. Saito, Y. Kohori, K. Kuga, Y. Matsumoto, S. Nakatsuji, H. Kito, P. M. Shirage, K. Kihou, N. Takeshita, C. H Lee, A Iyo, and H. Eisaki, "Possible multiple gap superconductivity with line nodes in heavily hole-doped superconductor KFe_2As_2 studied by ^{75}As nuclear quadrupole resonance and specific heat," J. Phys. Soc. Jpn. **78**, 083712 (2009).

[66] K. Hashimoto, A. Serafin, S. Tonegawa, R. Katsumata, R. Okazaki, T. Saito, H. Fukazawa, Y. Kohori, K. Kihou, C. H. Lee, A. Iyo, H. Eisaki, H. Ikeda, Y. Matsuda,

A. Carrington, and T. Shibauchi, "Evidence for superconducting gap nodes in the zone-centered hole bands of KFe_2As_2 from magnetic penetration-depth measurements," Phys. Rev. B **82**, 014526 (2010).

[67] J. P. Reid, M. A. Tanatar, A. Juneau-Fecteau, R. T. Gordon, S. R. de Cotret, N. Doiron-Leyraud, T. Saito, H. Fukazawa, Y. Kohori, K. Kihou, C. H. Lee, A. Iyo, H. Eisaki, R. Prozorov, and L. Taillefer, "Universal heat conduction in the iron arsenide superconductor KFe_2As_2: Evidence of a *d*-wave state," Phys. Rev. Lett. **109**, 087001 (2012).

[68] K. Okazaki, Y. Ota, Y. Kotani, W. Malaeb, Y. Ishida, T. Shimojima, T. Kiss, S. Watanabe, C.-T. Chen, K. Kihou, C. H. Lee, A. Iyo, H. Eisaki, T. Saito, H. Fukazawa, Y. Kohori, K. Hashimoto, T. Shibauchi, Y. Matsuda, H. Ikeda, H. Miyahara, R. Arita, A. Chainani, and S. Shin, "Octet-line node structure of superconducting order parameter in KFe_2As_2," Science **337**, 1314 (2012).

[69] S. Lederer, Y. Schattner, E. Berg, and S. A. Kivelson, "Enhancement of superconductivity near a nematic quantum critical point," Phys. Rev. Lett. **114**, 097001 (2015).

[70] J. Kang and R. M. Fernandes, "Superconductivity in FeSe thin films driven by the interplay between nematic fluctuations and spin-orbit coupling," Phys. Rev. Lett. **117**, 217003 (2016).